BLADE-VORTEX INTERACTION CAPTURE BY CFD

T. Renaud[*], G. Perez[**], C. Benoit[**], G. Jeanfaivre[**], S. Péron[**]

[*] ONERA, 8 rue des Vertugadins, 92190 Meudon, France
Email address: thomas.renaud@onera.fr
Phone number: (33) 1 46 73 42 40
Fax number: (33) 1 46 73 41 46

[**] ONERA, BP 72, 29 Avenue de la Division Leclerc, 92322 Châtillon, France

Abstract

For many years, the CFD simulation of the blade-vortex interaction has remained an important challenge as it requires an accurate capture and a long conservation of the blade tip vortex during the rotor revolution. In the framework of the French-German project SHANEL, the HART Baseline configuration of the BO105 rotor in descent flight has been studied. This paper deals more particularly with the validation of high-order accurate methods on Cartesian grids. In a first step, a mesh refinement is used to obtain a reference solution capturing BVI interactions on a fine grid. Then, high order schemes are applied on a coarser mesh in order to obtain the same level of accuracy concerning BVI capture. For the mesh refinement, the optimization of the meshing process is achieved through an automatic generation and adaptation of Cartesian background grids around the Chimera blade mesh. Among the different spatial schemes evaluated in this study, the 3rd order scheme with matrix dissipation provides the highest level of accuracy. The corresponding acoustic post-treatment of the CFD results correlates fairly well with the HART experiment, in terms of maximum noise level and directivity. Indeed, this high-order accurate method on Cartesian grid provides a maximum noise level, underestimated by only 1.7dB.

Introduction

This paper refers to a work accomplished in the French-German SHANEL (Simulation of Helicopter Aerodynamics Noise and ELasticity) project. The main purpose of this project is to apply numerical methods developed in different work packages for helicopter wakes conservation and interaction, such as rotor or fuselage configurations.
The present document deals in particular with the capture of the blade-vortex interaction (BVI) by CFD for a rotor in descent flight conditions. The numerical simulation of the flowfield around helicopter rotor blades remains a challenging problem. In particular, the interactions between the blades and the wake play a major role for performance, blade loads, vibrations and acoustics. These interactions are predominant in hover and in descent flight configurations when the wake below the rotor is swept away with low velocities. In these conditions, an accurate prediction of the wake geometry remains one of the most difficult problems in helicopter rotor aerodynamics.
Two approaches can be considered to predict blade-vortex interactions (BVI). On one side, the lifting line approach allowed obtaining good agreement with experiments for classical rotor geometries (BO105 rotor) thanks to a perfect conservation of the rotor wake but they are less accurate for complex geometries (ERATO rotor [1]). On the other side, CFD methods (Euler or Navier-Stokes) correctly predict the flowfield around almost any blade geometry but they are too diffusive for the wake simulation. In the framework of the French-German CHANCE cooperation (2001-2006), the Chimera techniques were developed and used for automatic mesh generation and adaptation in the *elsA* solver. In 2004, these methods were applied to the HART Baseline test-case, but no BVI was simulated due to too coarse blade and background grids.
In the framework of SHANEL, the objective of this new task is to capture the blade-vortex interaction with fine reference meshes and to improve the efficiency of the computations by applying advanced numerical methods (high-order schemes, vorticity confinement…). The CFD results will serve as input data for noise analysis and will be compared to the HART experimental measurements.

Numerical tools and configuration

The *elsA* solver

The main features of the *elsA* software [2][3] used in this work for simulating an unsteady

flow around rotating blades using the Chimera technique are described in this part.
In the present case, the *elsA* code solves the 3D compressible Euler equations in a blade attached rotating reference system. The spatial discretisation of the equations is achieved thanks to the space-centered Jameson's scheme. The 2nd and 4th order coefficients of the Jameson artificial viscosity are equal respectively to 0 and 0.016. The time integration is obtained with a four-stage Runge-Kutta explicit scheme and an IRS (Implicit Residual Smoothing) implicit phase. The constant time step corresponds to a variation of 0.1° of the azimuth per time step. It can also be noticed that an implicit Gear time integration or dual time stepping approach would not allow increasing the time step significantly because of the physical frequency around 30/rev of the BVI phenomenon. The Chimera method allows interpolating the solution between the child blade meshes and the background grid.

The Cassiopée tool

The Cassiopée tool [4][5] is an external module which is employed here to generate and refine automatically Cartesian background grids around the blades. On these particular grids, sophisticated methods such as higher order schemes or vorticity confinement are easier to develop and more efficient to resolve. In particular, the third order scheme is a correction of the classical Jameson scheme, using the same dissipation; in the flux discretization, the centered term is modified in order to achieve third order accuracy leading to a directional explicit scheme. Moreover, with this strategy, the background grid can be optimized so that the refinement indicator matches for example the rotational (curl) of the flowfield. The required CPU time and memory can also be decreased since operators can be simplified and no metrics storage is used for Cartesian grids. As before, the solutions are interpolated between the blade grids and the different levels of the background mesh.
It can be noticed that, in this first phase of SHANEL, the Cassiopée module has been used as a standalone tool, but in the future it will be coupled to the *elsA* solver for the curvilinear body grids in order to access to essential functionalities such as turbulence and transition models, low Mach number preconditioning…

Acoustics prediction methodology

The acoustics prediction methodology consists in a direct post treatment of CFD fields (density, velocity components, pressure) computed by *elsA*, by the KIM code [9] based on integral methods. For each acoustics computation, two formulations were used: the Ffowcs-Williams and Hawkings (FW-H) solid and porous surface formulations. These two different formulations, supposed to provide the same results, were used in order to check the consistency of CFD data. In particular, the comparison of the results given by these two formulations enabled us to check that the velocity fields computed by CFD computation was expressed in a reference frame coherent with the acoustics computation.

The BO105 blade grid

A particular attention has been paid to the generation of the blade grid. Indeed, even if the background grid is fine enough to conserve the rotor wake, the blade grid has also to be fine enough to avoid the dissipation of the vortices inside it and to capture a correct blade-vortex interaction.
A standard analytical method used for the generation of single-block grids around isolated blades is used for the generation of the child blade grids presented in Figure 1. Each blade grid contains 161x115x47=870205 points, so the four blades represent 3.48M points. A C-topology mesh has been chosen with a volume extension restricted to one blade chord. The mesh has been extended towards the root and the tip of the blade for the Chimera interpolations. 117 points describe the profile (chordwise) and 101 points are uniformly distributed along the spanwise direction. In this whole grid, the biggest cell size is equal to 0.13c.

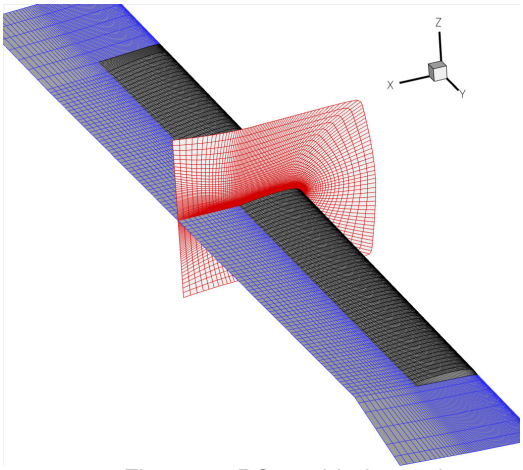

Figure 1 - BO105 blade mesh

The HART test case

The BO105 model rotor was tested in the DNW wind tunnel during the HART [6] and HART II [7] tests, whose objective was to analyze the influence of the Higher Harmonic Control to reduce the Blade-Vortex Interaction noise. The baseline configuration chosen for this computation corresponds to a descent flight with:

- the shaft incidence α_q=-4.2°,
- the advance ratio μ=0.15,
- the lift coefficient Zb=11.22,
- the tip Mach number MωR=0.635
- no High Harmonic Control.

The BO105 rotor has got four rectangular blades, equipped with NACA23012 airfoils. The blade aspect ratio is equal to 16.529 and the linear aerodynamic twist is equal to -8°/R, R being the blade radius equal to 2m.
In this first phase of SHANEL, the blade is assumed to be rigid (no elastic deformation) and the blade kinematics is imposed with respect to the Baseline HART experimental data (no coupling).

Reference computations

Description of the background grid

For the reference computations with *elsA*, the background grid generation was performed manually without Chimera overlapping between the blocks (Figure 2). The mesh extends up to 4.8R in each direction of the rotor plane and to 3.6R above and below it. The uniform Cartesian central block contains the BO105 rotor and is refined according to three levels of refinement:

- Coarse grid: Δh=0.3c
- Standard grid: Δh=0.15c
- Fine grid: Δh=0.075c

These different cell sizes correspond to a global background grid size of 3.65M, 8.05M and 27.9M points respectively.

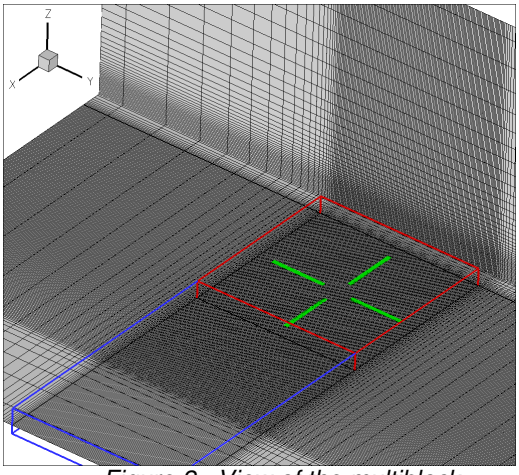

Figure 2 - View of the multiblock background grid

Effect of the mesh refinement

The CFD results were obtained after 5 rotor revolutions, which lead to a correct convergence of the computations, as Figure 3 and Figure 4 show respectively for the sectional load and rotor lift coefficients. Indeed, Figure 3 shows the sectional load C_ZM^2 at r/R=0.87 for the fine grid computation during the last 4 revolutions, with particular focuses on the advancing (Ψ=[0°-90°]) and the retreating sides (Ψ=[255°-345°]) where BVI occurs. The curves corresponding to the 4th and 5th revolutions differ only slightly for the amplitudes of some high frequency oscillations (Ψ=15°, 40°, 300°, 315°). These oscillations come from the blade-vortex interactions and demonstrate the ability of the simulation to capture the phenomenon. A more detailed comparison with the experiment is discussed further. In Figure 4, the good convergence can also be noted with the global evolution of the rotor lift coefficient Z_b and the effect of the mesh refinement during the last revolution: some high frequency peaks appear on the decreasing phase of the lift and their amplitude increases with the refinement. A small inflexion on the top of the lift curve for the smallest mesh cell size can also be noticed.

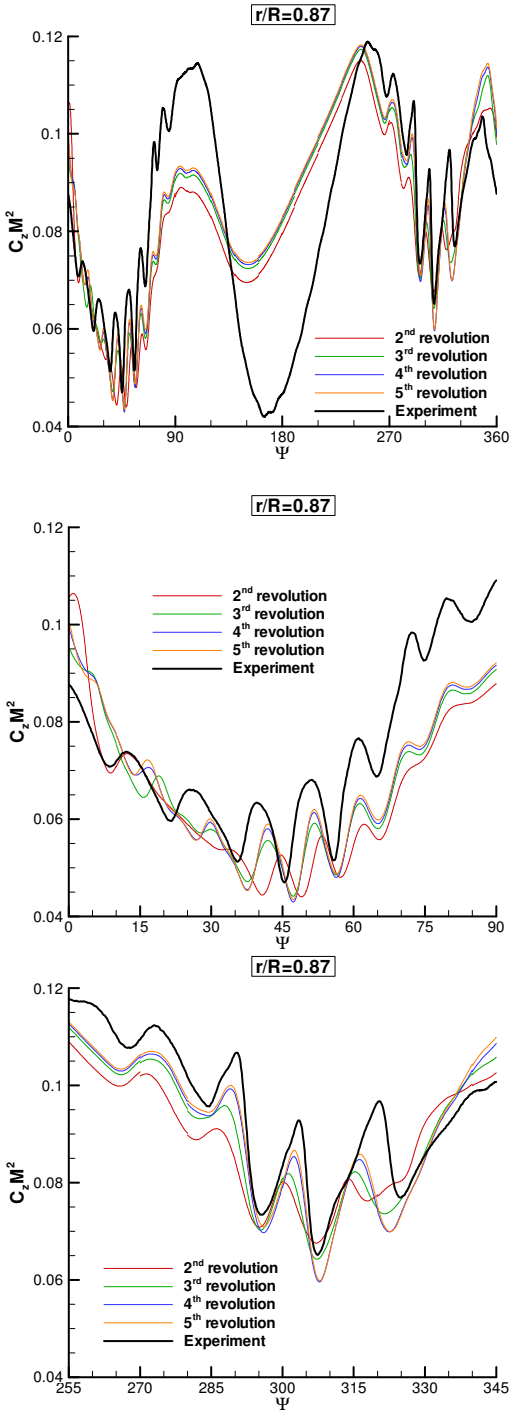

Figure 3 - Convergence of the sectional load C_ZM^2 for the fine background grid

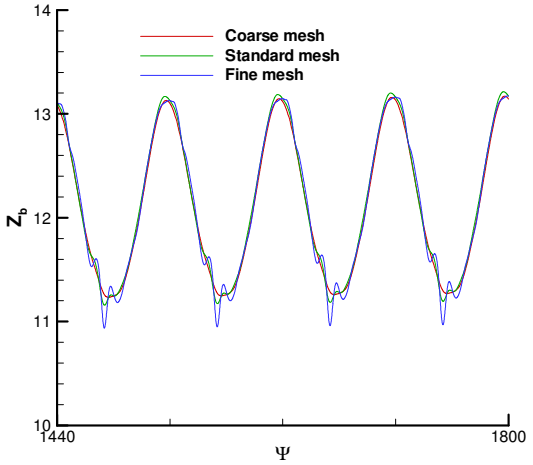

Figure 4 - Evolution of the rotor lift coefficient Z_b

Figure 5 presents the different wake solutions for the three levels of refinement of the background grid. For all figures, the iso-surface of Q-criteria (colored by the vorticity magnitude) has the same value (non-dimensional value of $Q=6.10^{-5}$):

$$Q = -\frac{1}{2}\frac{\partial V_i}{\partial x_j}\frac{\partial V_j}{\partial x_i}.$$

Obviously, the computed solution is more accurate when increasing the refinement: for the coarse grid, the blade tip vortex is conserved during ½ revolution, about one revolution for the standard grid and 1 ½ revolution for the finest one. In the last picture, the rolling up of the two rotor disk edge vortices can also be observed and a lot of small vortex structures are captured in particular in the BVI regions (first and fourth quadrants).

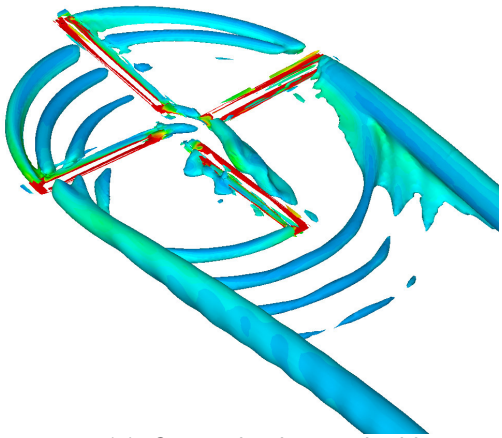

(a) Coarse background grid

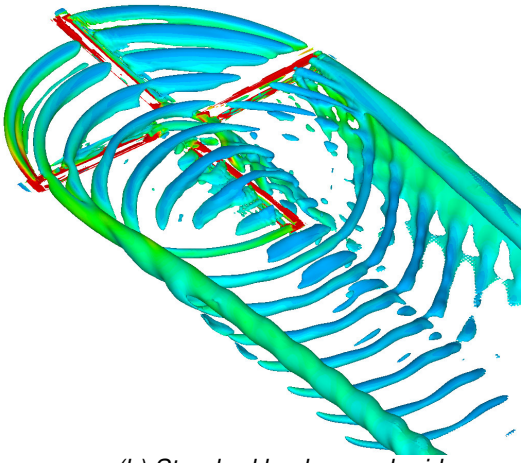

(b) Standard background grid

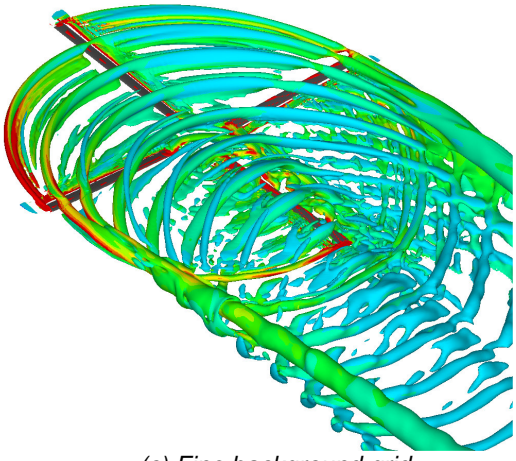

(c) Fine background grid

Figure 5 -Visualization of the rotor wake with the iso-surface of Q-criteria colored by vorticity magnitude

It is also interesting to follow the vortex locations from emission to interaction, as the BVI noise amplitude is directly linked to the position of the vortex with respect to the blade. That was one of the objectives of the HART II campaign, where PIV measurements were performed and post-processed [8]. Figure 6 presents the vortices location during their convection on the advancing and retreating sides for the Y=1.4m section. The standard and fine meshes solutions (the coarse one is not refined enough to locate any vortex) are compared to the PIV data for each position. Even if the computed altitudes (z-coordinate) are underestimated, the predicted trend is quite good and the fine mesh improves the results. In particular, for the positions 22, 23 and 46 (where the blade-vortex interactions occur), the numerical values are in good agreement with experiment.

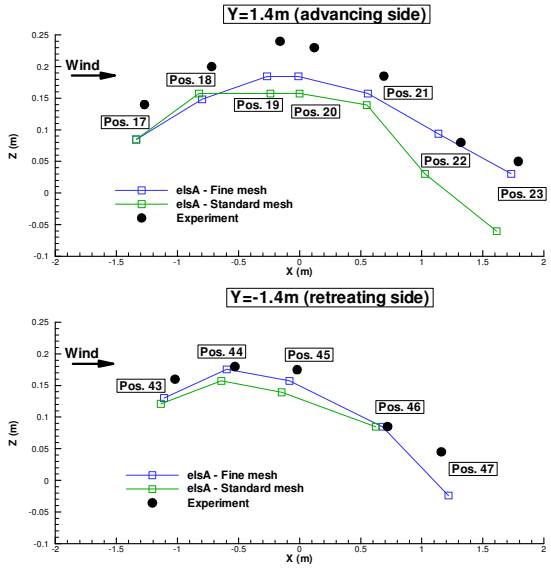

Figure 6 - Vortices location compared to PIV measurements

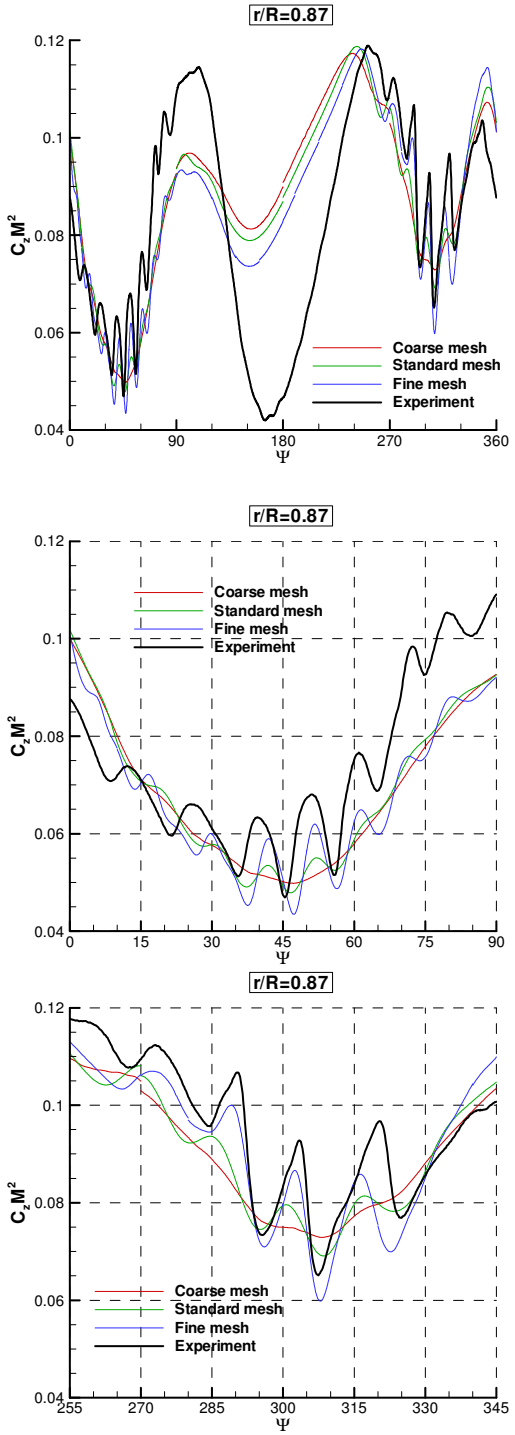

Figure 7 - Effect of grid refinement on the sectional load at r/R=0.87

In Figure 7, the sectional load is plotted versus azimuth at section r/R=0.87. The three computation results are compared to the HART experiment. The low frequency oscillation and the shape of the $C_Z M^2$ curves between 90° and 270° are not captured by CFD because of the rigid blade assumption. The coarse mesh is not fine enough to conserve the vortices and let them interact with the blades. With the standard grid, some BVI oscillations occur, in particular on the retreating side, but the amplitude and the slope of these oscillations are not strong enough with respect to experiment. The fine mesh improves significantly the solution, in terms of phase, amplitude and slope of the oscillations. Indeed, almost all BVI peaks are present on the advancing and retreating sides, although the phasing cannot be fully correct due to the rigid blade assumption.

Another way to analyze the results in terms of blade-vortex interactions is to compare the sectional load time derivative. Indeed, the slope of the sectional load oscillations corresponds to a pressure gradient which is the main source of the BVI noise. Figure 8 describes the distribution of this quantity on the rotor disk for the different numerical and experimental results, whereas Figure 9 presents its evolution with respect to the azimuth at section r/R=0.87. It can be noted that the blade-vortex interactions are not the same on the advancing and retreating sides. On the advancing side, the oscillations are more impulsive and extend more inboard along the blade. Moreover, there are more peaks in this region than on the retreating side, where the oscillations are less numerous and more spread. According to the fine mesh solution in Figure 8, it seems that the blade-vortex interactions do not have the same directivity: the vortex interactions are closer to parallel interactions on the advancing blade than on the retreating blade.

As seen before, the fine mesh improves noticeably the results in terms of BVI amplitudes and phases, but Figure 9 demonstrates also that the slope of the oscillations are quite well captured by CFD. However, the sectional load derivatives are still underestimated, in particular on the retreating side.

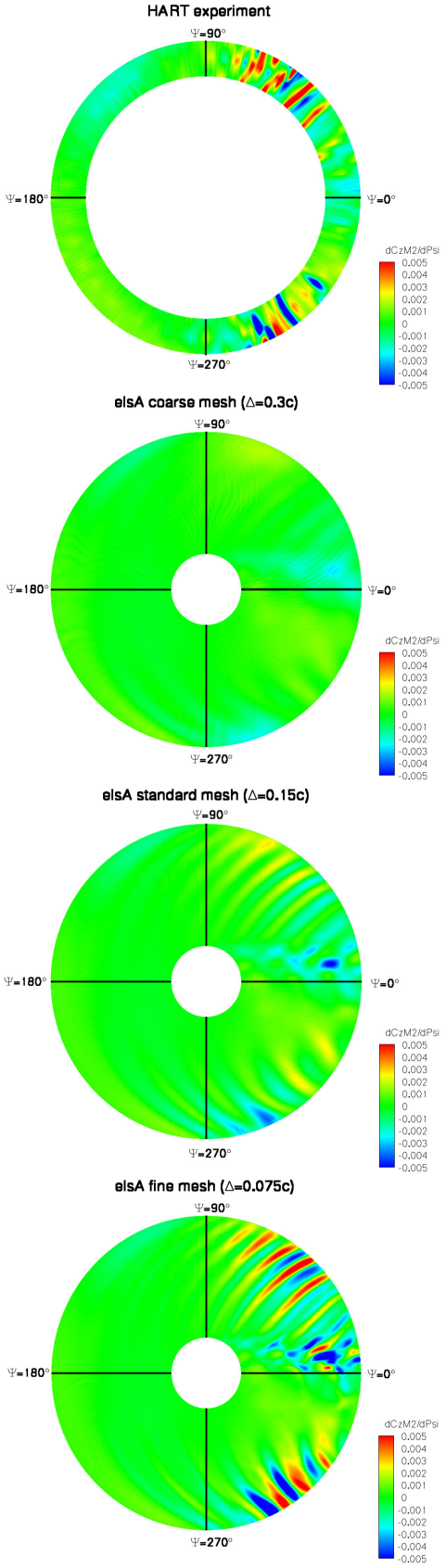

Figure 8 - Distribution of the sectional load derivative on the rotor disk

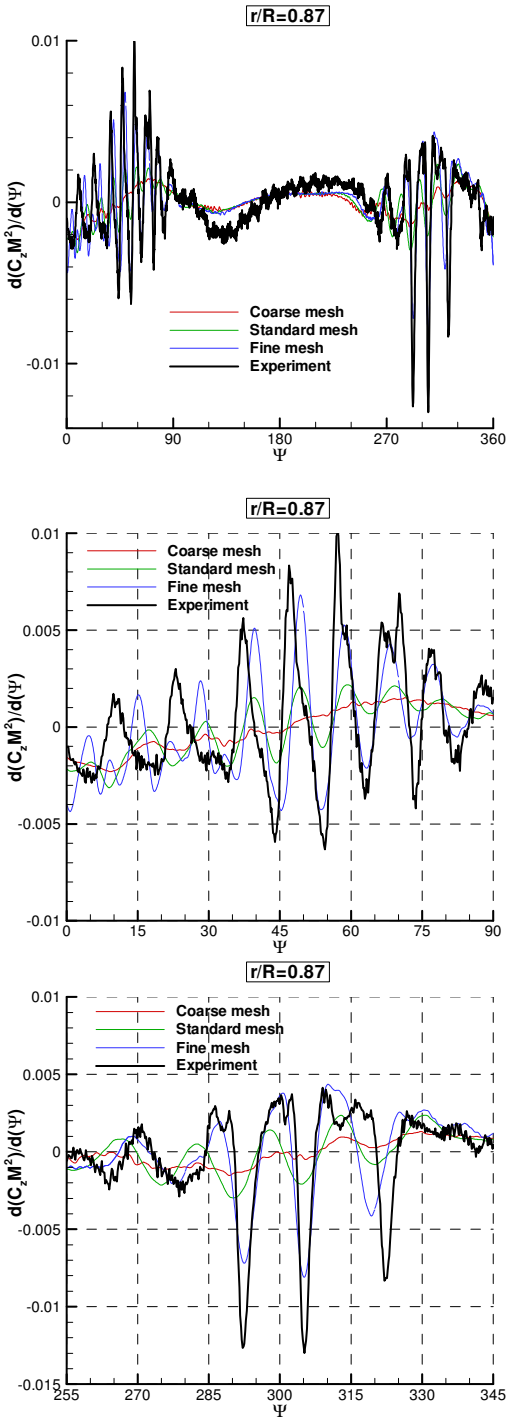

Figure 9 - Effect of grid refinement on the sectional load derivative at r/R=0.87

Acoustic analysis

As explained in the acoustic methodology section, for each computation two different formulations were used to check the consistency of the CFD data. For concision reasons, such a

comparison is only presented for the standard mesh computation. The acoustic signal at an observer location situated in the rotor plane (2.5R from the rotor centre) is computed with both formulations. The observer location was chosen in the rotor plane for the noise to be dominated by its thickness component. Since this component is linked to the fluid velocities on the blade surface, any inconsistency between the fluid and the blade motions (velocities given in an incorrect reference frame for instance) should lead to a significant discrepancy between the signals predicted by the two formulations. Figure 10 presents the corresponding results. A good agreement is found between the two different formulations, which ensures the consistency of the input data for acoustics.

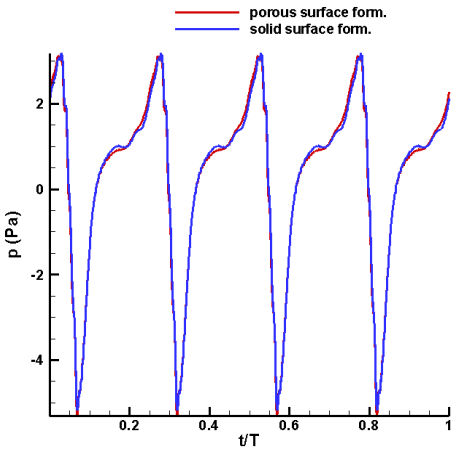

Figure 10 - Acoustic pressure signals predicted by FW-H solid and porous surface formulations

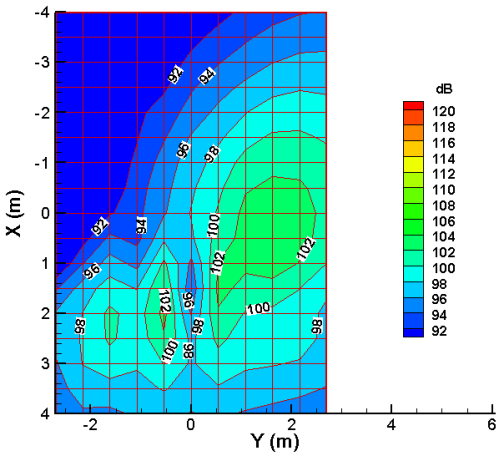

(a) standard mesh

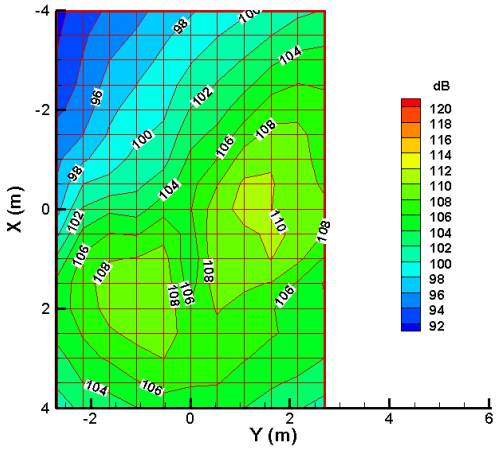

(b) fine mesh

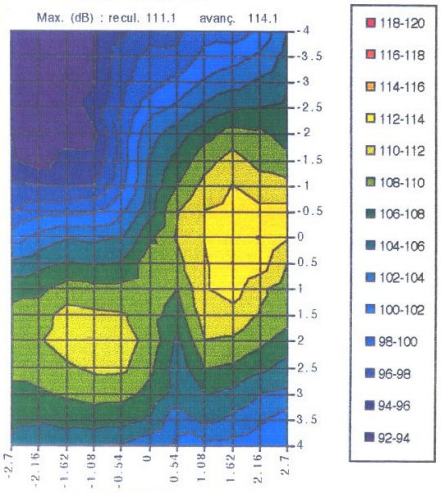

(c) experiment

Figure 11 - Comparison of the different predicted noise footprints. Noise levels filtered in (6-40 bpf) range

Once the validity of the acoustics computation established, one can present the noise

footprints corresponding to the standard and fine mesh spatial discretizations, which are presented in Figure 11. A 6-40 bpf filtering was applied to eliminate low frequency loading noise and make BVI noise emerge. As can be seen, the use of the fine grid clearly improves BVI noise prediction. The predicted maximum noise level increases by 6.9 dB while passing from the standard mesh to the fine grid. The under-estimation of this level has been drastically reduced with the finer discretization (standard: Δ=10.4 dB; fine: Δ=3.5 dB). We can also observe in this figure that the directivities on the advancing and retreating blade sides are well predicted, especially with the fine grid.

The fact that one obtains an acceptable prediction of BVI noise levels with the finer discretization tends to prove that the vortex diffusion is limited with this mesh. Actually, even if the BVI intensity depends on other parameters (miss-distance, interaction parallelism), the vortex core size is a key factor determining BVI noise amplitude. The discrepancy between predicted and measured maximum noise levels would be greater if the numerical diffusion led to non-physical values of the vortex core size. The analysis of the predicted noise spectra, that will give us more insight in the predicted BVI physics, will enable us to draw a more definitive conclusion on the predicted vortex core size.

The good agreement between predicted and measured noise directivities is consistent with the good prediction of wake geometry established in Figure 6.

Improvement of the computations

As seen in the previous part, the BVI phenomenon can be correctly captured by CFD with a fine mesh, as the blade-vortex interactions seem to depend only on a good convection (in terms of maintaining the intensity of the vortices during a long time) and location of the vortices. Consequently, the next part of the work deals with attempts to improve the simulations using more advanced numerical methods. As described before, the Cassiopée module allows generating Cartesian background grids, for which the CPU effort will be decreased, as no “ghost cells” or metrics have to be calculated. Moreover, thanks to the automatic mesh generation and refinement, the total number of points may be optimally adapted to the rotor wake. In the first phase of SHANEL, recent developments of numerical methods are applied to the BVI test case.

Cartesian meshes

The same standard level of refinement (Δh=0.15c) as for the *elsA* reference computations is used here for the automatic Cartesian grid generation. The main difference with the previous computations is that the final grid is obtained after several automatic refinements with respect to the Q criteria. The meshing process was stopped after that the whole rotor disk was refined in order to adapt to the vortex till its interaction with the blade. Finally, the standard background grid contains about 6M points which represents a decrease of 25% of the total number of points with respect to the reference standard mesh. Figure 12 shows the different steps and the final mesh obtained for the standard refinement level.

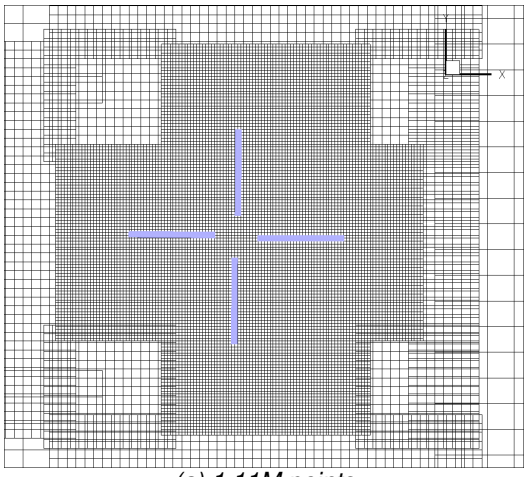

(a) 1.11M points

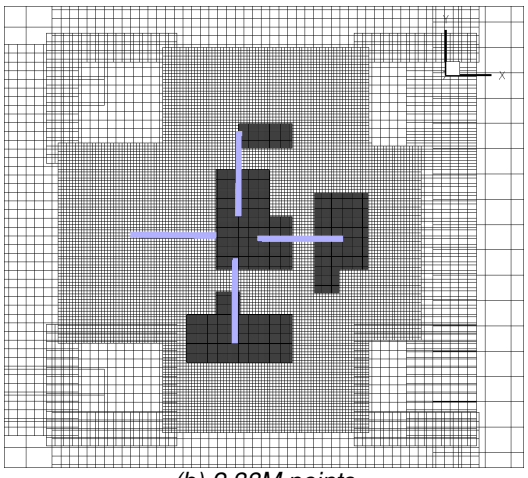

(b) 2.38M points

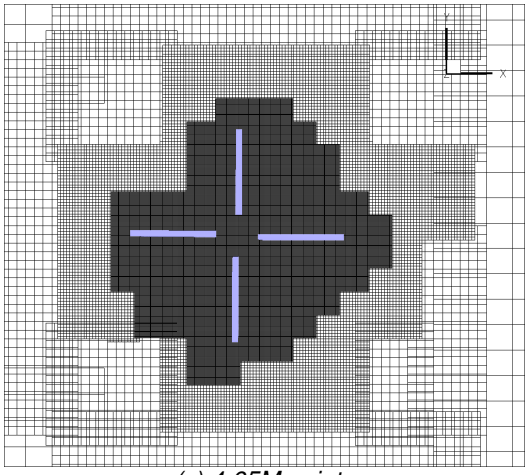

(c) 4.65M points

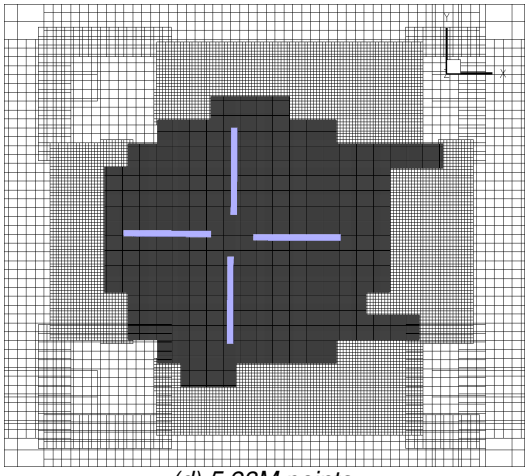

(d) 5.93M points

Figure 12 - Automatic Cartesian grids for the standard cell size

Effects of the numerical scheme

In Figure 13, the effect of the numerical scheme is analyzed for the standard Cartesian mesh solution. The sectional load $C_Z M^2$ at r/R=0.87 is plotted for 4 computations including: the 2nd order scheme, the 2nd order scheme and the matrix dissipation, the 3rd order scheme, the 3rd order scheme and the matrix dissipation. In fact, the Jameson scheme leads to the resolution of a matrix system, which can be simplified with the scalar approximation of the dissipation and may lead to a larger numerical diffusion. That is why the matrix representation of the dissipation has been tested on the Cartesian background grid (the scalar dissipation is still used on the curvilinear blade grids) in order to improve the vortex convection. In the reference computations with *elsA*, a lack of robustness of this matrix dissipation on the blade grids prevents us from using the matrix dissipation, and contrary to Cassiopée, it is not possible to use different numerical parameters on different grid blocks. As can be seen on these results, the matrix dissipation has a very significant effect on the solution, in particular on the amplitude of BVI oscillations. For this standard grid, the order of the scheme has less influence on the results, with only a slight improvement of the phase of the BVI oscillations. Finally, the solution obtained with the 3rd order scheme and the matrix dissipation with this standard Cartesian grid compares very well with the HART experiment. Surprisingly, the matrix dissipation with the 2nd order scheme removes the BVI on the retreating side, while it is still efficient on the advancing side: this point has to be clarified. Table 1 provides the CPU time consumption of the different computations, performed on 16 Intel Itanium 2 Montecito processors. The additional cost due to the matrix dissipation is 2.4% for the 2nd order scheme and 1.7% for the 3rd order one, whereas the CPU time is increased by 18% with the use of the 3rd order scheme with respect to the 2nd order one.

Numerical method on standard grid	2nd order	2nd order with matrix diss.	3rd order	3rd order with matrix diss.
CPU time (16 processors) µs/pt/iter	2.50	2.56	2.96	3.01

Table 1 - CPU time comparison for the different numerical methods

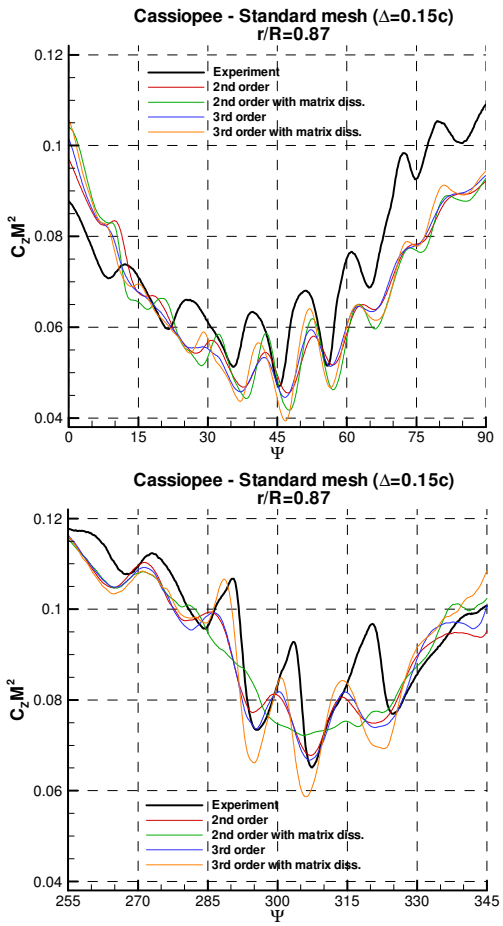

Figure 13 - Effect of the numerical method on the sectional load at r/R=0.87

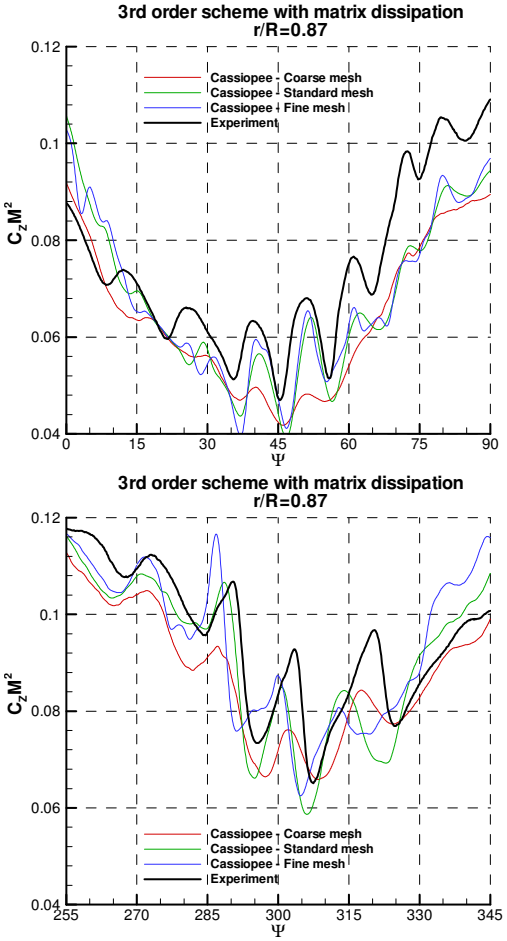

Figure 14 - Effect of the grid refinement on the sectional load with a 3rd order scheme and matrix diss.

Grid convergence with high-order scheme

It is known that the behavior of the numerical methods can depend on the mesh refinement and it is interesting to investigate how the 3rd order scheme with matrix dissipation behaves on a finer grid. Figure 14 and Figure 15 show the effect of grid refinement for the 3rd order scheme with matrix dissipation. The sectional load and its derivative are plotted on the advancing and retreating sides at r/R=0.87.
The discrepancies between the standard and the fine grids solutions are weak. The grid refinement and the numerical method have both similar but not additive effects on the solution, i.e. a better location of the vortices (presence of all BVI peaks) and a better conservation of their intensity (more impulsive oscillations).

Finally, by comparing respectively Figure 7 and Figure 14 or Figure 9 and Figure 15, the solutions given by the 3rd order scheme with matrix dissipation on a standard grid and the 2nd order scheme on a fine grid are very similar. Of course, the additional CPU time cost due to the 3rd order scheme and the matrix dissipation is less than the extra CPU time due to a finer mesh. Indeed, the Cassiopée computation on the standard grid requires 28.3h CPU time for one rotor revolution (on 16 processors), whereas the *elsA* computation on the fine grid requires 265h CPU time.

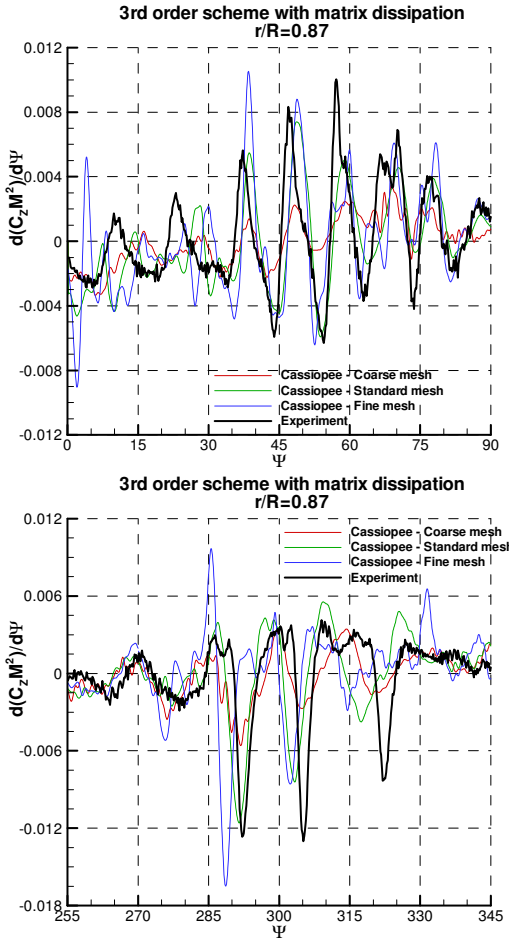

Figure 15 - Effect of the grid refinement on the sectional load derivative with a 3rd order scheme and matrix diss.

<u>Acoustic analysis</u>

The noise footprints corresponding to the three different schemes are presented in Figure 16. Again, a 6-40 bpf filtering was applied to eliminate low frequency loading noise and make BVI noise emerge.

As can be seen, the use of the third order scheme with scalar dissipation only leads to a moderate improvement of the noise level prediction compared to the 2nd order reference scheme (scalar dissipation). The under-estimation of the maximum noise level has been reduced by 3.5 dB (2nd order: Δ=10.4 dB; 3rd order with scalar dissipation: Δ=6.9 dB). The use of the 3rd order scheme with matrix dissipation (c) leads to a clear improvement of the BVI noise prediction compared to the reference (a). With this scheme, the under-estimation of the maximum noise level has been drastically reduced (reduction: 8.7 dB) and the predicted maximum noise level is close to the measured value (Δ=1.7 dB).

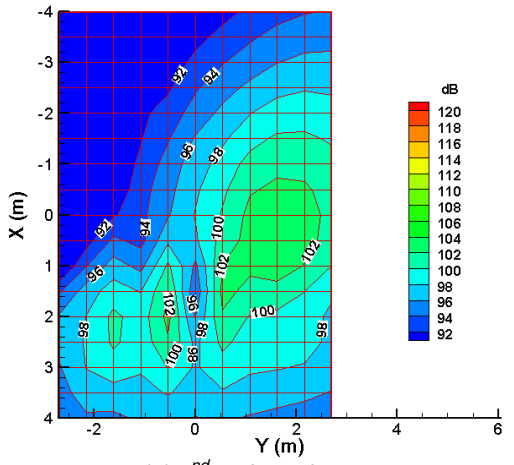

(a) 2nd order scheme

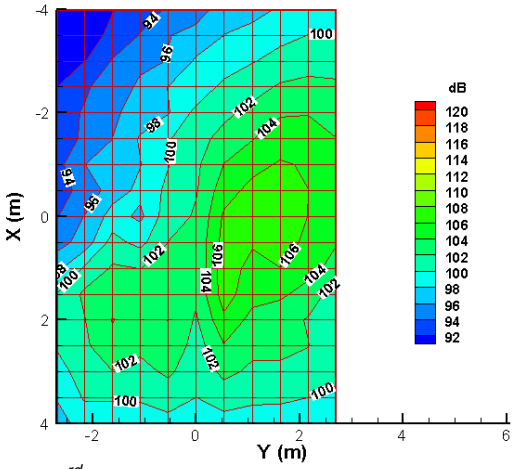

(b) 3rd order scheme with scalar dissipation

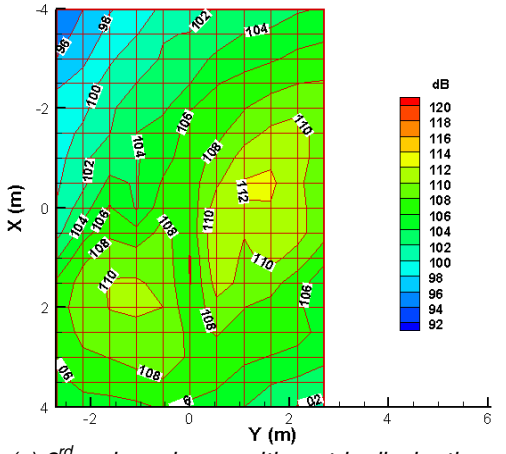

(c) 3rd order scheme with matrix dissipation

Figure 16 - Comparison of the different predicted noise footprints. Noise levels filtered in (6-40 bpf) range

The fact that one obtains a good prediction of BVI noise levels in Figure 16c tends to prove

that the vortex diffusion is limited with this scheme.
In order to qualify in further details the prediction characteristics, the acoustic pressure signals were analysed. The comparison of the predicted signals to the measured ones will enable us to determine whether the physics of BVI is well captured by the computation. For this comparison (Figure 17) we consider the computation with the 3rd order scheme with matrix dissipation which provided the most accurate prediction of noise levels.

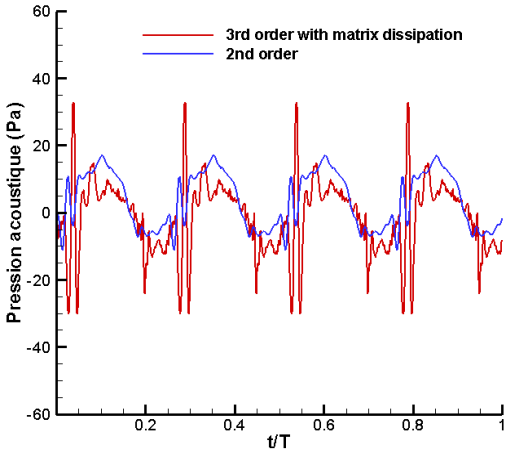

(a) Predictions

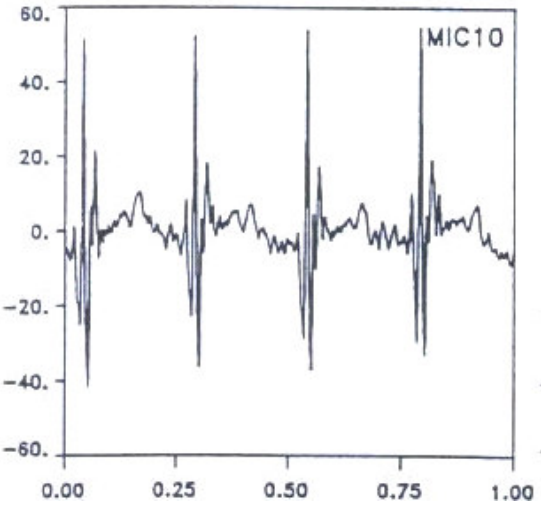

(b) Experiment

Figure 17 - Comparison of the predicted acoustic pressure signals (a) to the experimental one (b).

Although the peak to peak amplitude of the main BVI event is under-predicted, one can observe that the physics of BVI is well captured with the 3rd scheme with matrix dissipation: the number and relative amplitude of the predicted BVI peaks matches the experiment for the advancing side interactions.

Conclusion and perspectives

In the first phase of the SHANEL project, the objective was to simulate the HART BVI test-case by the first applications of recent numerical developments. During this work, reference computations have been performed with the *elsA* solver. They demonstrated the ability of the code to simulate with a good accuracy the blade-vortex interactions with the use of a 31.4M points mesh. The use of a fine mesh improved significantly the prediction of the maximum noise level compared to results obtained on a standard mesh. The under-prediction of this maximum level was reduced by 6.9 dB (standard: Δ=10.4 dB; fine: Δ=3.5 dB).
The Cassiopée module, which allows automatically generating and refining Cartesian background grids around the rotor and using sophisticated methods (high-order schemes, matrix dissipation, Vorticity Confinement), was also applied to the BVI problem. This technique proved to be efficient for the BVI capture, as a computation on a 9.4M points grid with a 3rd order scheme and matrix dissipation leads to results comparable with the reference solution and in good agreement with the HART experiment: all the BVI oscillations of sectional loads are captured with correct amplitudes and sometimes underestimated slopes. A good prediction of noise levels and directivity was obtained for both advancing and retreating side interactions. The maximum noise level was only under-predicted by 1.7 dB.
In the second phase of the SHANEL project, the effort on validation of the numerical methods (5th order scheme, Vorticity Confinement) will be maintained. The present results can also be improved by taking into account the blade elasticity and by coupling the CFD code with a comprehensive analysis, in particular for the Minimum Noise and Minimum Vibration test-cases with HHC. New acoustic post-treatments of *elsA* CFD fields will be performed. The CFD computations will also be used to study the vortex roll-up phase and improve the corresponding model in the code MENTHE.

Acknowledgements

The authors would like to acknowledge the French Ministry of Transport DPAC for the financial support of the numerical studies presented in this paper. The technical management of this project is done by the French Ministry of Defence DGA.

References

[1] Prieur J., Splettstoesser W. R., *ERATO: an ONERA-DLR cooperative programme on aeroacoustic rotor optimisation*, 25th European Rotorcraft Forum, Rome, Italy, September 14-16, 1999.

[2] Cambier L., Gazaix M., *elsA: an efficient object-oriented solution to CFD complexity*, 40th AIAA Aerospace Science Meeting and Exhibit, Reno, USA, January 2002.

[3] Cambier L., Veuillot J. P., *Status of the elsA CFD software for flow simulation and multidisciplinary applications*, 48th AIAA Aerospace Science Meeting and Exhibit, Reno, USA, January 7-10, 2008.

[4] Benoit C., Jeanfaivre G., *3D inviscid isolated rotor and fuselage calculations using Chimera and automatic Cartesian partitioning methods*, Journal of the American Helicopter Society, pp. 128-138, April 2003.

[5] Saunier O., Benoit C., Jeanfaivre G., Lerat A., *Third-order Cartesian overset mesh adaptation for solving steady compressible flows*, International Journal for Numerical Methods in Fluids, November 2007.

[6] Yu Y. H., Gmelin B., Heller H., Philippe J. J., Mercker E., Preisser J. S., *HHC aeroacoustics rotor test at DNW – The joint German/French/US HART project*, 20th European Rotorcraft Forum, Amsterdam, Netherlands, September 1994.

[7] Yu Y. H., Tung C., van der Wall B. G., Pausder H., Burley C., Brooks T., Beaumier P., Delrieux Y., Mercker E., Pengel K., *The HART-II test: rotor wakes and aeroacoustics with higher-harmonic pitch control (HHC) inputs – The joint German/French/Dutch/US project*, American Helicopter Society 58th Annual Forum, Montreal, Canada, June 11-13, 2002.

[8] Bailly J., Delrieux Y., Beaumier P., *HART II : experimental analysis and validation of ONERA methodology for the prediction of blade-vortex interaction*, 30th European Rotorcraft Forum, Marseille, France, September 2004.

[9] Rahier G. and Zibi J., *A Fast Kirchhoff Integration Technique for Rotor Noise Directivity Predictions*, 55th Annual Forum of the American Helicopter Society, Montreal Canada, May 1999.